Contemporary Mathematics
http://ojs.wiserpub.com/index.php/CM/

UNIVERSAL WISER PUBLISHER

Research Article

Host Viral Load During Triple Coinfection of SARS-CoV-2, Influenza Virus, and Syncytial Virus

Mesfin Asfaw Taye

Science Division, West Los Angeles College, 9000 Overland Ave, Culver City, CA 90230, USA
Email: tayem@wlac.edu

Received: 14 February 2023; **Revised:** 18 March 2023; **Accepted:** 22 March 2023

Abstract: The dynamics of the host viral load during triple coinfection between severe acute respiratory syndrome coronavirus 2 (SARS-CoV-2), influenza A, and the syncytial virus is studied. To explore how the host cells, the infected cells, and the viral load behave as a function of time, numerical simulations are performed. Via numerical simulations, the differential equations are analyzed by considering initial conditions. Since the numerical simulations are performed by using the physiological parameters, the model system can genuinely help to understand the viral dynamics either in vivo or in vitro. The result obtained in this work depicts that a higher viral load is exhibited when the three viruses simultaneously infect the host cells than in a single infection case. This indicates that simultaneous infection with SARS-CoV-2, influenza A, and syncytial viruses might be associated with a higher morbidity and mortality rate as these viruses by cooperating with each other facilitate a higher infection rate. Using physiological parameters, we further study the correlation between viral load, susceptible cells, and infected cells. As the three viral species cooperatively infect the host cells, the number of infected cells rises resulting in a higher viral load. Since influenza A has a higher viral reproduction rate than the two types of virus, it dictates the overall dynamics as it has a competitive advantage. Since these viruses share the same resources, the virus production of a given virus can be affected by the other. The interference of these viruses relies on the initial dose, the order of infection, and the strain of the virus. We show that when influenza A and syncytial viruses are initiated a few days after SARS-CoV-2 establishes an infection, while SARS-CoV-2 thrives, and the other two viruses fail to establish an infection. The viruses with an initially higher dose have also a survival advantage. Furthermore, the effect of lymphocytes on the overall viral dynamics is explored via numerical simulations. Since SARS-CoV-2 targets several types of cells and organs, a higher SARS-CoV-2 viral load can be also associated with a higher morbidity and mortality rate.

***Keywords*:** MERS-CoV, SARS-CoV-2, COVID-19, mathematical model, immune system, basic reproduction number

MSC: 92C12

1. Introduction

Since SARS-CoV-2, influenza A virus (IAV), and syncytial virus are respiratory viruses, they exhibit similar clinical symptoms such as running nose, fever, cough, and congestion. The severe acute respiratory disease syndrome

DOI: https://doi.org/10.37256/cm.4320232500

coronavirus 2 (SARS-CoV-2 or COVID-19) not only killed millions of people across the globe but also cost a trillion dollars globally. After the virus was isolated from patients from Wuhan, Hubei Province, China in the year 2019 [1], the disease quickly spreads across the globe despite several pharmaceutical measures. The IAV on the other hand affects millions of people every year and as a result, it becomes a constant public threat. Similar to SARS-CoV-2 and IAV, the respiratory syncytial virus (RSV) infects the respiratory tract and it is one of the global health concerns. Being ribonucleic acid (RNA) viruses, SARS-CoV-2, influenza, and syncytial viruses mutate during replications. Due to a lack of proofreading, these viruses evolve through time resisting the available vaccines and antiviral therapies. Their continuous existence causes high morbidity and mortality worldwide every year.

As SARS-CoV-2, IAV, and syncytial virus, have overlapping seasons, patients can be simultaneously infected by multiple viruses. For instance, public health officials in California recently urged preventive measures against the triple threat of SARS-CoV-2, influenza, and syncytial viruses since these viruses can simultaneously infect individuals. In order to understand the viral dynamics in the presence of multiple infections, several models have been proposed [2-8]. Since these viruses share the same resources, the virus production of a given virus can be affected by the other. The interference of these viruses relies on the initial dose, the order of infection, and the strain of the virus. As a result, the viruses can interfere either constructively (synergistically) or destructively (inhibitory).

The interference of viruses during coinfection has been the subject of many studies. The study by Goto et. al. indicates that human parainfluenza viruses (PIV) can facilitate the growth of IAV since these viruses interfere constructively [9]. On the other hand, RSV may interfere with IAV by inhibiting protein synthesis [10]. As indicated by the work [10], by abating immune response, RSV helps the spread of IAV. On the contrary, Shinjoh et. al. indicates that IAV can be suppressed by RSV if the infection by RSV is initiated before IAV [11]. A fast-growing virus such as rhinovirus reduces replication of all other respiratory viruses [12]. Coinfection of SARS-CoV-2 with other respiratory viruses is more common in pediatric patients than in adult patients [13-15]. The clinical effect of coinfection is still debated. Some studies indicate that the coinfection of influenza with SARS-CoV-2 has fewer impacts [16] while other studies show that the two viruses interact destructively and as a result, the coinfection leads to a lower mortality rate. On the contrary other studies also suggest that both viruses interact constructively in some patients causing a higher virus production rate. This also implies that the coinfection between SARS-CoV-2, IAV, and RSV might cause high morbidity and mortality rate [12-17]. In particular, SARS-CoV-2 not only infects epithelial cells but also infects lymphocytes as a secondary target. This in turn might weaken the immune response and help the spread of other viruses. The discrepancy in these results can be resolved via a mathematical model.

Mathematical models serve as a basic tool to study the dynamics of the virus within the host cells in vivo by Hernandez-Vargas et al. [7] or in vitro [18-32]. By solving the model system either numerically or analytically, the dynamics of the target cells as well as the viral load can be explored as a function of time. The effect of the immune response on the overall viral load can be also explored efficiently via mathematical models. The viral dynamic models were originally adapted from epidemiological models as a result they share similar features. The epidemiological models focus on the infection dynamics at the population level while the viral dynamics models concentrate on the host cells level. Often mathematical models effectively describe the infection dynamics and help to predict the severity of a given virus. In the last few decades, several mathematical model systems have been developed to study the dynamics of hepatitis C virus (HCV) [33-36], human immunodeficiency virus (HIV) [18-28, 37-39] as well as influenza viruses [40, 41]. In the effort to understand the dynamics of COVID-19, several mathematical models have been also considered. For instance, the interaction between SARS-CoV-2, the target cells, and the host immune system was discussed in the works [8]. The role of natural killer cells and T-cells in the SARS-CoV-2 dynamics was studied in the work [42]. The study by Wang et al. indicates that during SARS-CoV-2 infection the viral load steps up monotonously and attends a plateau phase after reaching its peak. As time evolves, the viral load decreases due to the adaptive immune system [8]. The effect of initial viral load as well as the order of infection on the severity of infection was studied by Hernandez-Vargas et al. [7].

In this work, the dynamics of the host viral load during triple coinfection between SARS-CoV-2, influenza A, and the syncytial viruses are studied. To explore how the host cells, the infected cells, and the viral load behave as a function of time, numerical simulations are performed. Via numerical simulations, the differential equations (1) are analyzed by considering initial conditions. Since the numerical simulations are performed by using the physiological parameters depicted in Table 1, our model system can genuinely help to understand the viral dynamics either in vivo or in vitro.

In modeling the viral dynamics, it is vital to consider the role of natural killer cells as well as T cells. The natural killer cells, being part of the innate immune system, act as first-hand protection. More comprehensive protection is granted by T cells. Not only do they tackle viral growth, but also participate in removing the virus from the host. In this work, we study the effect of the lymphocytes on the overall viral dynamics.

The new result obtained in this work also exhibits that a higher viral load is exhibited when the three viruses simultaneously infect the hot cells than in a single infection case which indicates that simultaneous infection with SARS-CoV-2, influenza A, and the syncytial virus can be associated with a higher morbidity and mortality rate as these viruses by cooperating with each other facilitate a higher infection rate. Using physiological parameters, the correlation between viral load, susceptible cells, and infected cells is explored. We show that when the three viral species cooperatively infect the host cells, a higher viral load is observed. The overall dynamics are dictated by the IAV since it has a higher viral reproduction rate than the two types of virus. The virus production of a given virus can be affected by others since these viruses share the same resources. The interference of these viruses relies on the initial dose, the order of infection, and the strain of the virus. The main result of this paper depicts that when influenza A and syncytial viruses are initiated a few days after SARS-CoV-2 establishes an infection, while SARS-CoV-2 thrives, and the other two viruses fail to establish an infection. The initial viral load also significantly affects the overall dynamics. The viruses with an initially higher dose have also a survival advantage. Furthermore, the effect of lymphocytes on the overall viral dynamics is explored via numerical simulations. Since SARS-CoV-2 targets several types of cells, a higher SARS-CoV-2 viral load can be also associated with a higher morbidity and mortality rate. Furthermore, different from other respiratory viruses, SARS-CoV-2 infects the upper respiratory tract, lower respiratory tract, nervous system, gastrointestinal system, and other organs such as the kidney. Therefore, even though SARS-CoV-2 has the lowest viral replication rate, by infecting several organs, its viral load can be considerably large. The initial viral dose and the timing of infection might have little effect since even if the infection in one organ is blocked by another virus, SARS-CoV-2 can flourish in other organs. Patients infected by COVID-19 develop acute respiratory distress and the virus destroys cells and tissues. As a result, at any viral load, infection with SARS-CoV-2 results in higher mortality and morbidity rate in the unvaccinated patient.

The rest of the paper is organized as follows: in Section 2 and Section 3, we study the dynamics of viruses in the presence of triple coinfection. In Section 4, the dependence of viral load on the model parameters is explored by including the effect of lymphocytes. Section 5 deals with the summary and conclusion.

2. The confection between COVID-19, IAV and RSV

Throughout human history, respiratory viruses such as human bocavirus (hBoV), adenovirus (AdV), PIV, coronavirus (CoV), human metapneumovirus (hMPV), influenza B virus (IBV), IAV, human enterovirus (hEV), human rhinovirus (hRV) and RSV have impacted human civilization. Since these viruses concurrently infect the same host, they interact either constructively or destructively depending on the initial inocula, the viral strain, and the time of infection. The dynamics of these viruses can be studied via mathematical models.

As discussed before, the mathematical models serve as a basic tool to study the dynamics of the virus within the host cells. By solving the model system either numerically or analytically, the dynamics of the target cells as well as the viral load can be explored as a function of time. The effect of the immune response on the overall viral load can be explored efficiently via mathematical models. The mathematical model proposed in this work is adapted from the previous works [11, 43]. In the model system, the three most common pathogenic viruses simultaneously infect the epithelial cells (see Figure 1) based on the model equations:

$$
\begin{aligned}
\dot{T} &= -\beta_1 T V_1 - \beta_2 T V_2 - \beta_3 T V_3,\\
\dot{E}_1 &= \beta_1 T V_1 - k_1 E_1 - E_1 \beta_2 V_2 - E_1 \beta_3 V_3,\\
\dot{I}_1 &= k_1 E_1 - \delta_1 I_1,\\
\dot{V}_1 &= p_1 I_1 - c_1 V_1,\\
\dot{E}_2 &= \beta_2 T V_2 - k_2 E_2 - E_2 \beta_1 V_1 - E_2 \beta_3 V_3,\\
\dot{I}_2 &= k_2 E_2 - \delta_2 I_2,\\
\dot{V}_2 &= p_2 I_2 - c_2 V_2,\\
\dot{E}_3 &= \beta_3 T V_3 - k_3 E_3 - E_3 \beta_1 V_1 - E_3 \beta_2 V_2,\\
\dot{I}_3 &= k_3 E_3 - \delta_3 I_3,\\
\dot{V}_3 &= p_3 I_3 - c_3 V_3.
\end{aligned} \tag{1}
$$

Here, T denotes the population of the epithelial cells, the SARS-CoV-2 virus V_1, the IAV V_2 and the RSV V_3 infect T at the rates of β_1, β_2 and β_3, respectively. Throughout the paper, it is assumed that a given virus infects only one cell. E_1, E_2 and E_3 represent the eclipse phase for SARS-CoV-2, IAV, and RSV, respectively. At this stage, the virus can not release viral components. The cells at the eclipse phase become infectious at the rate of k_1, k_2, and k_3 where I_1, I_2, and I_3 represent infectious cells for SARS-CoV-2, IAV, and RSV, respectively. The cells remain infectious for periods which are given by $1/\delta_1$, $1/\delta_2$ and $1/\delta_3$. The SARS-CoV-2, IAV, and RSV are produced at rates p_1, p_2 and p_3 and become cleared at the rates of c_1, c_2 and c_3 as shown in Table 1. The role of immune response is not considered. In addition to respiratory epithelial cells, the SARS-CoV-2 is known to infect the T lymphocytes. In this work, the dynamics of host cells, virus load, and infected cells as a function of time t will be studied by considering initial conditions $T(0) > 0$, $E_1(0) > 0$, $E_2(0) > 0$, $E_3(0) > 0$, $V_1(0) > 0$, $V_2(0) > 0$, and $V_3(0) > 0$.

Table 1. Experimental data for COVID-19, IAV and RSV [11]

Virus	B ($[V]^{-1}d^{-1}$)	k (d^{-1})	δ (d^{-1})	p ($[V]^{-1}d^{-1}$)	c (d^{-1})
COVID-19	7.5×10^{-7}	4.2	0.06	2.9×10^{4}	19
RSV	2.85×10^{-7}	4.2	4.2	3.47×10^{9}	4.03
IAV	2.7×10^{-5}	1.27	1.27	8.71×10^{6}	1.27

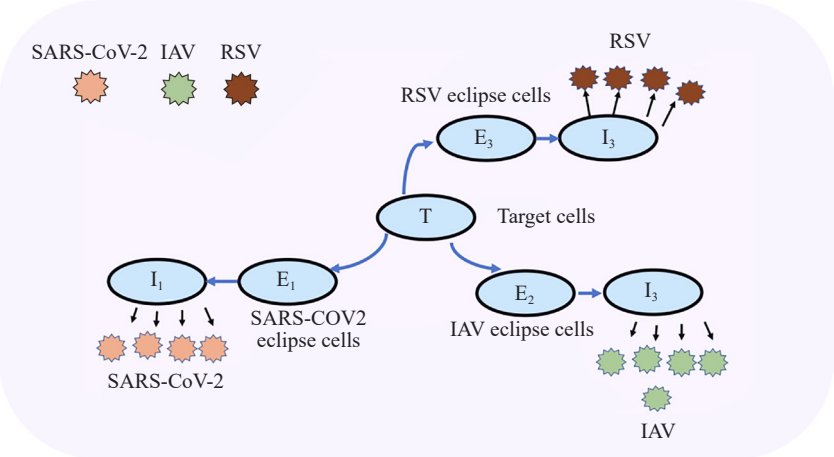

Figure 1. Schematic diagram showing triple coinfection of SARS-CoV-2, influenza virus, and syncytial virus.

In the next section, we study the dynamics of viruses during confection neglecting the role of natural killer cells as well as T cells.

To understand how these respiratory viruses dominate each other through time, it is instructive to analyze the ratio of the viral load of a given strain of virus to the total viral load. The total viral load is given by $\Sigma_i^3(V_i)$. The ratio of viral load is given as

$$\begin{aligned}\varsigma_1 &= \frac{V_1}{\sum_i^3 (V_i)},\\ \varsigma_2 &= \frac{V_2}{\sum_i^3 (V_i)},\\ \varsigma_3 &= \frac{V_3}{\sum_i^3 (V_i)},\end{aligned} \tag{2}$$

where ζ_1, ζ_2, and ζ_3 are the ratio of the viral load for SARS-CoV-2, IAV and RSV, respectively. Similarly, the ratio of the eclipse cells that are infected by a given strain of virus to the total eclipse cells is denoted as

$$\begin{aligned}\psi_1 &= \frac{E_1}{\sum_i^3 (E_i)},\\ \psi_2 &= \frac{E_2}{\sum_i^3 (E_i)},\\ \psi_3 &= \frac{E_3}{\sum_i^3 (E_i)},\end{aligned} \tag{3}$$

where ψ_1, ψ_2, and ψ_3 denote the ratio of the eclipse cells of SARS-CoV-2, IAV and RSV, respectively. The ratio of the infected cell by a specific viral type to the total infected cells is given by

$$\begin{aligned}\pi_1 &= \frac{I_1}{\sum_i^3 (I_i)},\\ \pi_2 &= \frac{I_2}{\sum_i^3 (I_i)},\\ \pi_3 &= \frac{I_3}{\sum_i^3 (I_i)},\end{aligned} \tag{4}$$

where π_1, π_2, and π_3 are the ratio of the infectious cells of SARS-CoV-2, IAV and RSV, respectively.

2.1 *Case 1: The coinfection between SARS-CoV-2 and IAV*

While clinical data indicates coinfection of two or more viruses is more common in pediatric patients than adult patients, its clinical effect is still debated. When influenza and SARS-CoV-2 concurrently infect the host, some studies suggest that the coinfection of influenza with SARS-CoV-2 has fewer impacts [13-15] while other studies show that the two viruses interact destructively and as a result, the coinfection leads to a lower mortality rate [16]. In case of confection between SARS-CoV-2 and IAV, the dynamics of host cells, infected cells and viral load are given by

$$
\begin{aligned}
\dot{T} &= -\beta_1 T V_1 - \beta_2 T V_2,\\
\dot{E}_1 &= \beta_1 T V_1 - k_1 E_1 - E_1 \beta_2 V_2,\\
\dot{I}_1 &= k_1 E_1 - \delta_1 I_1,\\
\dot{V}_1 &= p_1 I_1 - c_1 V_1,\\
\dot{E}_2 &= \beta_2 T V_2 - k_2 E_2 - E_2 \beta_1 V_1,\\
\dot{I}_2 &= k_2 E_2 - \delta_2 I_2,\\
\dot{V}_2 &= p_2 I_2 - c_2 V_2.
\end{aligned} \tag{5}
$$

where T denotes the host cell. E_1 and E_2 designate the eclipse cells for the SARS-CoV-2 and IAV, respectively. I_1 and I_2 represent the infected cells for the SARS-CoV-2 and IAV, respectively. The virus load for SARS-CoV-2 and IAV is denoted by V_1 and V_2.

The equilibrium abundance of the host cells, infected cells, and viral load can be given as

$$
\begin{aligned}
\dot{T}^* &= \frac{c_1 c_2 \delta_1 \delta_2 (k_1 + k_2)}{\beta_1 c_2 \delta_2 k_1 p_1 + \beta_2 c_1 \delta_1 k_2 p_2},\\
\dot{E}_1^* &= \frac{-\beta_1 c_1 c_2 \delta_1 \delta_2 k_2 p_1 + \beta_2 c_1^2 \delta_1^2 k_2 p_2}{\beta_1 p_1 (\beta_1 c_2 \delta_2 k_1 p_1 + \beta_2 c_1 \delta_1 k_2 p_2)},\\
\dot{I}_1^* &= \frac{-\beta_1 c_1 c_2 \delta_2 \delta_1 k_2 p_1 + \beta_2 c_1^2 \delta_1 k_1 k_2 p_2}{\beta_1 p_1 (\beta_1 c_2 \delta_2 k_1 p_1 + \beta_2 c_1 \delta_1 k_2 p_2)},\\
\dot{V}_1^* &= \frac{-\beta_1 c_2 \delta_2 k_1 k_2 p_1 + \beta_2 c_1 \delta_1 k_1 k_2 p_2}{\beta_1 (\beta_1 c_2 \delta_2 k_1 p_1 + \beta_2 c_1 \delta_1 k_2 p_2)},\\
\dot{E}_2^* &= \frac{c_2 \delta_2 k_1 (\beta_1 c_2 \delta_2 p_1 - \beta_2 c_1 \delta_1 p_2)}{\beta_2 p_2 (\beta_1 c_2 \delta_2 k_1 p_1 + \beta_2 c_1 \delta_1 k_2 p_2)},\\
\dot{I}_2^* &= \frac{c_2 k_1 k_2 (\beta_1 c_2 \delta_2 p_1 - \beta_2 c_1 \delta_1 p_2)}{\beta_2 p_2 (\beta_1 c_2 \delta_2 k_1 p_1 + \beta_2 c_1 \delta_1 k_2 p_2)},\\
\dot{V}_2^* &= \frac{-\beta_1 c_2 \delta_2 k_1 k_2 p_1 + \beta_2 c_1 \delta_1 k_1 k_2 p_2}{\beta_1 (\beta_1 c_2 \delta_2 k_1 p_1 + \beta_2 c_1 \delta_1 k_2 p_2)}.
\end{aligned} \tag{6}
$$

The ratio $\frac{\dot{V}_2^*}{\dot{V}_1^*} = -\frac{\beta_1}{\beta_2}$. The ratio $\frac{\dot{E}_2^*}{\dot{E}_1^*} = -\frac{\beta_1 c_2 \delta_2 k_1 p_1}{\beta_2 c_1 \delta_1 k_2 p_2}$. The ratio $\frac{\dot{I}_2^*}{\dot{I}_1^*} = -\frac{\beta_1 c_2 p_1}{\beta_2 c_1 p_2}$. The equilibrium abundance of the uninfected cells steps up.

Consistent with the previous model system [11], first neglecting the terms $E_1\beta_2V_2$ and $E_1\beta_2V_2$, let us next explore how the number of host cells T, the number of infected cells I and the viral load V behave as a function of time by exploiting Equation (2) numerically. Throughout the papers, all of the physiological parameters are considered to vary per unit of time (days). In all figures, SARS-CoV-2, IAV, and syncytial viruses are denoted as COVID-19, IAV and RSV.

To explore how the host cells, the infected cells, and the viral load behave as a function of time, numerical simulations are performed. Via numerical simulations, the differential equations (2) are analyzed by considering initial conditions. Since the numerical simulations are performed by using the physiological parameters depicted in Table 1, our model system can genuinely help to understand the viral dynamics either in vivo or in vitro. Let us consider a single infection case (in the absence of coinfection). Since IAV has a higher viral infection rate p_2, it has the shortest infection time (it decays fast). On the other hand, SARS-CoV-2 is infectious for a longer period as it has a lower viral infection rate p_2 as shown in Figures 2a and 2b. The figures also depict that the viral load increases and attains a maximum value. As time evolves, the viral load decreases. since the viral infection rate of SARS-CoV-2 is significantly lower than IAV, the viral load for SARS-CoV-2 is significantly lower than IAV.

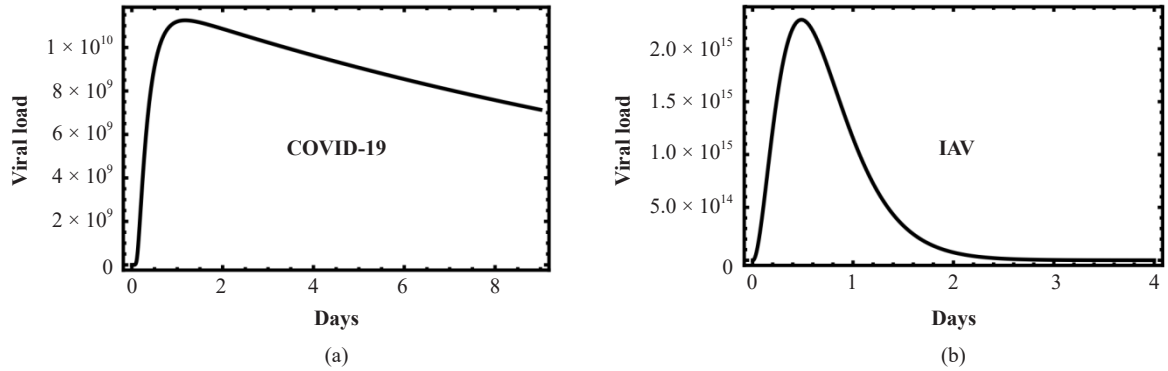

Figure 2. (a) SARS-CoV-2 viral load as a function of time (single infection). (b) IAV viral load vs time (single infection). Both figures depict that IAV has the shortest infection time (it decays fast). SARS-CoV-2 is infectious for a longer period as it has a lower viral infection rate. For the two viruses, the viral load increases and attains a maximum value. As time evolves, the viral load decreases. Since the viral infection rate for SARS-CoV-2 is significantly lower than IAV, the viral load for SARS-CoV-2 is significantly lower than IAV. In the figures, $T(0) = 10{,}000{,}000$, $V_1(0) = 100{,}000$ and $V_2(0) = 100{,}000$.

When SARS-CoV-2 and IAV concurrently target the host cells, they compete for the same cellular resources. As a result, they exhibit fascinating dynamics. In Figure 3a, the ratio of the infectious cells that are infected by a given strain of virus to the total infectious cells is plotted as a function of time. Here, π_1 and π_2 denote the ratio of the infectious cells of SARS-CoV-2 and IAV, respectively. Figure 3b depicts the ratio of viral load for a given virus to the total viral load as a function of time where ζ_1 and ζ_2 indicate the viral load for SARS-CoV-2 and IAV, respectively. The simulation results (see Figures 3a and 3b) indicates that since SARS-CoV-2 has a lower reproduction rate, its growth is considerably inhibited by IAV. Since IAV reproduces fast, it consumes most of cellular resources than SARS-CoV-2. However, since their combined viral load is higher than a single infection case, our model predicts that the coinfection by SARS-CoV-2 and IAV might cause higher morbidity or mortality in the unvaccinated patients.

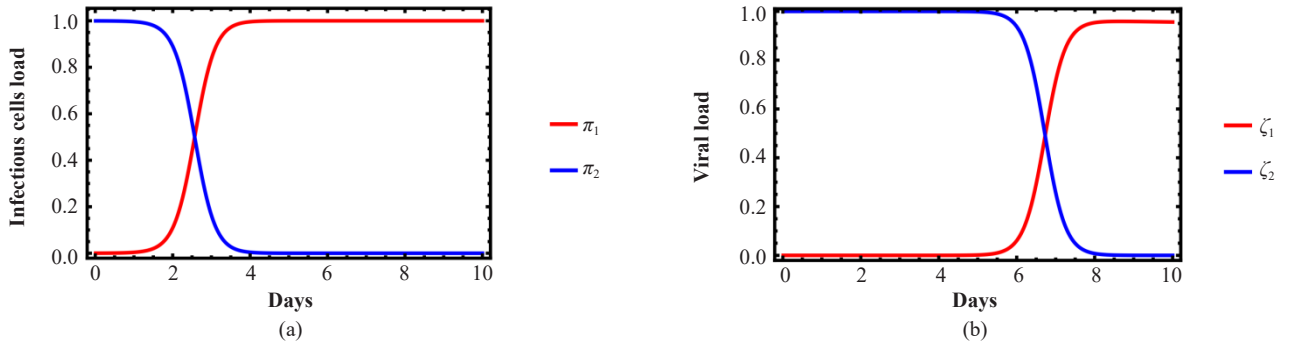

Figure 3. (a) The ratio of the infectious cells that are infected by a given strain of virus to the total infectious cells as a function of time. π_1 and π_2 denote the ratio of the infectious cells of SARS-CoV-2 and IAV, respectively. (b) The ratio of viral load for a given virus to the total viral load as a function of time. ζ_1 and ζ_2 indicate the viral load for SARS-CoV-2 and IAV, respectively.The two figures show that the SARS-CoV-2 viral load is considerably lower than IAV. In the figure, we fix $T(0) = 10{,}000{,}000$, $V_1(0) = 100{,}000$ and $V_2(0) = 100{,}000$.

The ratio of the infectious cells is plotted in Figure 4a. Figure 4b depicts the ratio of viral load as a function of time. Since the viruses are competing for the same cellular resources, the first virus that establishes an infection has a survival advantage. As depicted in the figures, since IAV is initiated 5 days after SARS-CoV-2 establishes an infection, SARS-CoV-2 consumes most of the cellular resources by infecting most of the cells. Consequently, IAV decays without causing an infection as shown in Figures 4a, 4b, and Figure 5.

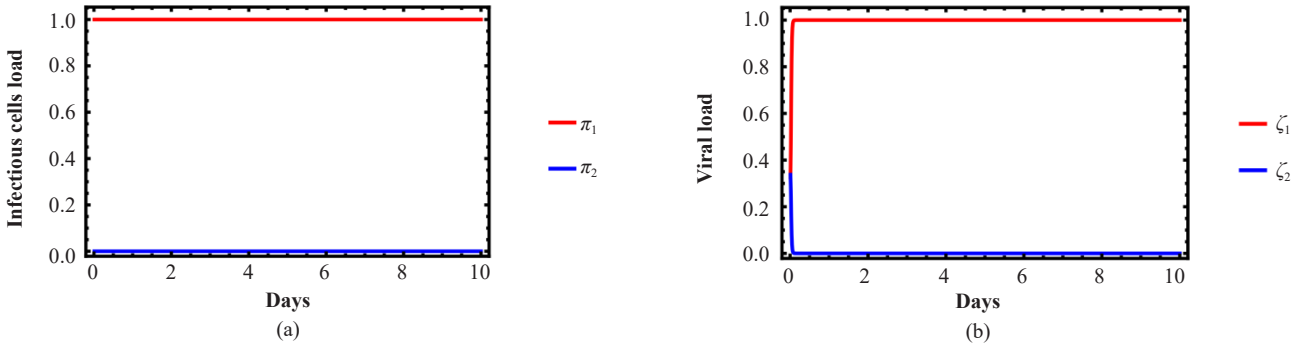

Figure 4. (a) The ratio of infected cells as a function of time when SARS-CoV-2 establishes an infection five days before IAV. (b) The ratio of viral load when IAV is initiated five days after SARS-CoV-2 establishes an infection. Because SARS-CoV-2 consumes most of the cellular resources by infecting most of the cells, IAV decays without causing an infection. In the figures, $T(0) = 10{,}000{,}000$, $V_1(0) = 100{,}000$ and $V_2(0) = 100{,}000$. In the figures, π_1 and π_2 denote the ratio of the infectious cells of the SARS-CoV-2 and IAV, respectively while ζ_1 and ζ_2 indicate the viral load for the SARS-CoV-2 and IAV, respectively.

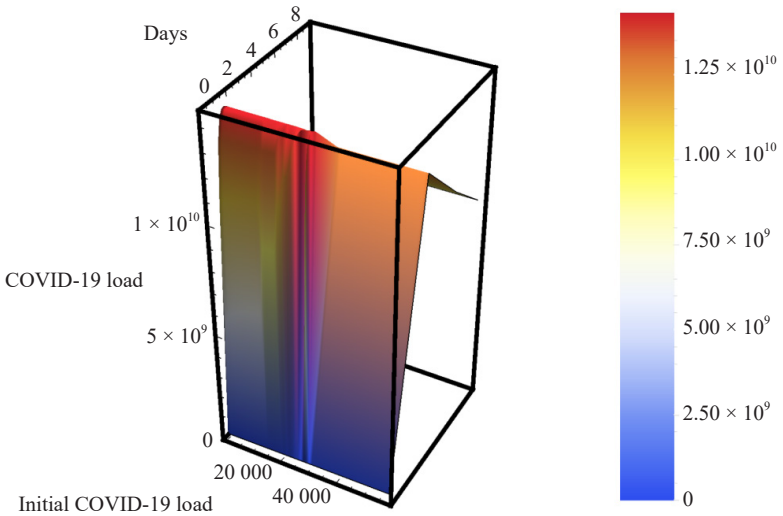

Figure 5. SARS-CoV-2 viral load as a function of time and initial IAV viral inoculum, when IAV is initiated five days after SARS-CoV-2, establishes an infection. The figure shows that since IAV is initiated 5 days after SARS-CoV-2, establishes an infection, SARS-CoV-2 consumes most of the cellular resources by infecting most of the cells. Consequently, IAV decays without causing an infection.

The initial viral load also significantly alters the infection dynamics as shown in Figure 6. In the figure, the initial viral inoculum for SARS-CoV-2 is vired by fixing the initial IAV viral inoculum. The figure depicts that the IAV viral load declines as the initial SARS-CoV-2 load steps up. A higher initial viral load facilitates more cellular infection when the infection starts. As time goes on, the fast-growing virus can infect more target cells.

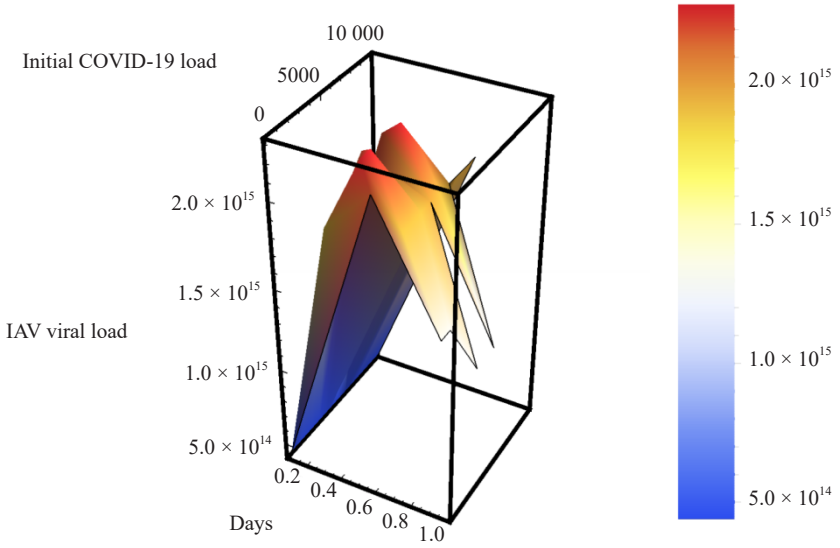

Figure 6. IAV viral load as a function of time and initial SARS-CoV-2 viral inoculum.

3. Triple coinfection

Most of the previous investigations were focused only on the coinfections of two viral species. In reality, the host cells can be infected by several viral species concurrently. In this section, we proposed a triple infection model where SARS-CoV-2, influenza A, and syncytial viruses interact simultaneously by sharing the cellular resources of the host cells. We solve the model system via numerical simulation.

When the cell is coinfected by SARS-CoV-2, IAV, and RSV, the infected cells I_1, I_2 and I_3 as well as the viral loads V_1, V_2 and V_3 exhibit intriguing dynamics. To explore how the host cells, the infected cells, and the viral load behave as a function of time, numerical simulations are performed. Via numerical simulations, the differential equations (2) are analyzed by considering initial conditions. As depicted in Figures 7a, 7b, and 7c, when SARS-CoV-2, RSV, and IAV concurrently target the host cells, they compete for the same cellular resources. The same figures show that IAV has a competitive advantage over the RSV and SARS-CoV-2 since it has a higher viral infection rate. RSV on the other hand has a higher infection rate than SARS-CoV-2 which implies that SARS-CoV-2 stays infectious for a longer period than the other two viruses. IAV has the highest viral load and decays fast. RSV also depicts a higher viral load than SARS-CoV-2. Since these viruses infect simultaneously the cell yielding a higher viral load than a single infection case, this triple coinfection might be associated with higher mobility.

To get a better insight, we analyze the ratio of infectious cells π_1, π_2 and π_3 as a function of time in Figure 8a. The ratio of varial load ζ_1, ζ_2 and ζ_3 as a function of time is plotted in Figure 8b during simultaneous infection of SARS-CoV-2, IAV, and RSV. Once again, as depicted in Figures 8a and 8b, IAV is highly competitive over a short time. On the contrary, a slow-reproducing virus (SARS-CoV-2) has a competitive advantage over the other two viruses in a long time limit. Even if an infection is over, a person can shed the virus for a longer period.

When the IAV infections are initiated after five days of SARS-CoV-2 infection and RSV is initiated one day after SARS-CoV-2 establishes an infection, SARS-CoV-2 becomes dominant only for a short period as the virus within a short period can infect more target cells. The fast-growing virus (IAV) quickly takes over and governs the overall dynamics in a long time limit as shown in Figure 9. The computation for cellular resources is the main factor in determining the viral load of a given virus. The dynamics of the virus is also determined by the initial viral inoculum. A virus with the highest viral load becomes dominant for a short period.

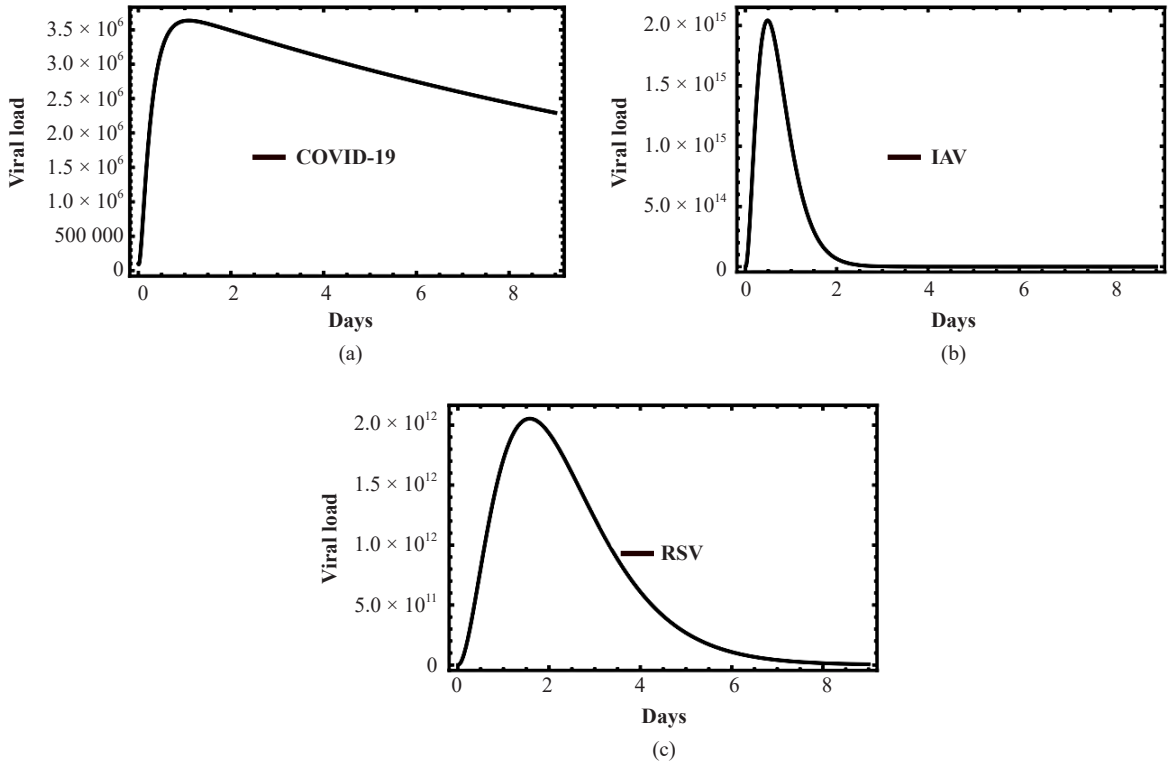

Figure 7. (a) SARS-CoV-2 viral load as a function of time. (b) IAV viral load as a function of time. (c) RSV viral load as a function of time. The three viruses simultaneously infect the target cells. In the figures, $T(0) = 10{,}000{,}000$, $V_1(0) = 100{,}000$, $V_2(0) = 100{,}000$ and $V_3(0) = 100{,}000$. As shown in the figures, when SARS-CoV-2, RSV, and IAV concurrently target the host cells, they compete for the same cellular resources. The same figures show that IAV has a competitive advantage over RSV and SARS-CoV-2 since it has a higher viral infection rate. RSV on the other hand has a higher infection rate than SARS-CoV-2 which implies that SARS-CoV-2 stays infectious for a longer period than the other two viruses.

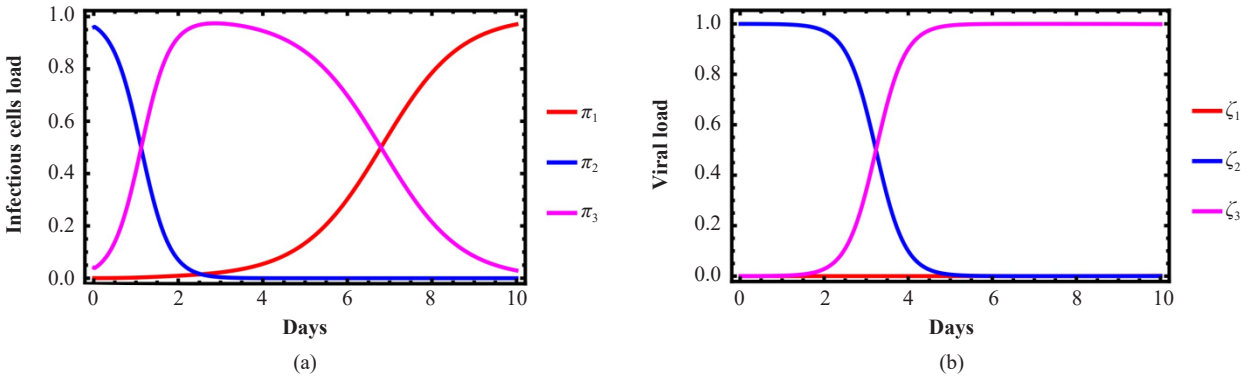

Figure 8. (a) The ratio of infectious cells π_1, π_2 and π_3 as a function of time. (b) The ratio of varial load ζ_1, ζ_2 and ζ_3 as a function of time during simultaneous infection of SARS-CoV-2, IAV, and RSV. The figures depict that IAV is highly competitive over a short time. On the contrary, SARS-CoV-2 has a competitive advantage over the other two viruses in a long time limit.

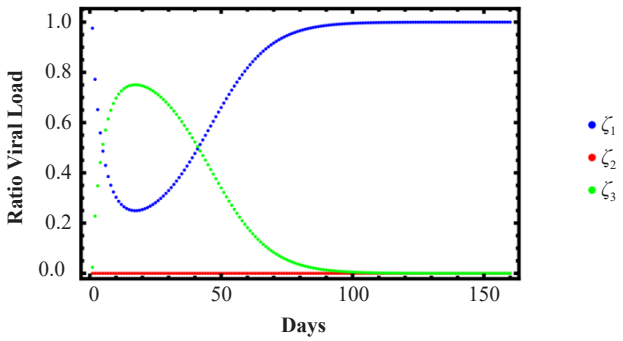

Figure 9. The ratio of varial load ζ_1, ζ_2 and ζ_3 as a function of time for concurrent infection when IAV is initiated five days after SARS-CoV-2 establishes an infection and RSV is initiated one day after SARS-CoV-2 establishes an infection. In this case, SARS-CoV-2 becomes dominant only for a short period as the virus within a short period can infect more target cells. The fast-growing virus (IAV) quickly takes over and governs the overall dynamics within a long time limit.

At this point, we want to stress that viruses use their cellular machinery and resources to reproduce. After the replication, the new virus particles leave the cell. This viral shedding is vital for the virus to complete its infection cycle. The duration of this viral shading depends on the type of variant and the host immune system. Different studies show that patients can shed SARS-CoV-2 till 60 days after symptom onset [44]. Children can also shed the viruses even for a longer period.

4. The triple confection in the presence of secondary target cells

As discussed before, most of the previous works studied the coinfection between two viruses. In this work, we proposed a new triple viral model which helps to study how the interaction between SARS-CoV-2, influenza A, and syncytial viruses affects the mortality and morbidity rate. The numerical simulation method is used as an alternative approach since our mathematical model is too complex to be solved analytically. The numerical simulation helps to study how the viral load for the three viruses behaves as a function of time.

In modeling the viral dynamics, it is vital to consider the role of natural killer cells as well as T cells. The natural killer cells, being part of the innate immune system, act as first-hand protection. More comprehensive protection is granted by T cells. Not only do they tackle viral growth, but also participate in removing the virus from the host. Some studies indicate the presence of viral particles of SARS-CoV and MERS-CoV in the lymphocytes [8, 42] which justifies that SARS-CoV-2 not only infects respiratory epithelial cells but also infects T lymphocytes. As discussed before, the plot of viral load as a function of time depicts a plateau phase which also serves as a piece of evidence that the lymphocytes are targeted by the virus [8]. Clinical data of patients who are infected by SARS-CoV-2 exhibits lymphocytopenia, particularly in severely ill patients. All of these scientific researches show that SARS-CoV-2 causes cytoplasmic damage by infecting lymphocytes and it maintains its survival by attracting the lymphocytes to the lung. Thus, in this model system, we study the viral dynamics by including lymphocytes as a secondary target. In this case, the basic model can be written as:

$$
\begin{aligned}
\dot{T} &= -\beta_1 T V_1 - \beta_2 T V_2 - \beta_3 T V_3,\\
\dot{E}_1 &= \beta_1 T V_1 - k_1 E_1 - E_1\beta_2 V_2 - E_1\beta_3 V_3,\\
\dot{L}_1 &= \lambda - \beta_1 L_1 V_1,\\
\dot{I}_1 &= k_1(E_1 + L_1) - (\delta_1 + \omega L_1) I_1,\\
\dot{V}_1 &= p_1 I_1 - c_1 V_1,\\
\dot{E}_2 &= \beta_2 T V_2 - k_2 E_2 - E_2\beta_1 V_1 - E_2\beta_3 V_3,\\
\dot{I}_2 &= k_2 E_2 - \delta_2 I_2,\\
\dot{V}_2 &= p_2 I_2 - c_2 V_2,\\
\dot{E}_3 &= \beta_3 T V_3 - k_3 E_3 - E_3\beta_1 V_1 - E_3\beta_2 V_2,\\
\dot{I}_3 &= k_3 E_3 - \delta_3 I_3,\\
\dot{V}_3 &= p_3 I_3 - c_3 V_3.
\end{aligned} \tag{7}
$$

Here, L_1 represents the concentration of lymphocytes. Hereafter, we considered it to be constant and to avoid mathematical complexity, we assume that lymphocytes and epithelial cells are infected by the SARS-CoV-2 virus at the same rate. For simplicity, the eclipse phase is not considered for the lymphocytes L_1. The parameters λ and ω are fixed as $\lambda = 10^4$ day^{-1} and $\omega = 2.9 \times 10^{-4}$ [41]. To simplify the model system, the infection rate β_1 is assumed to be the same for lymphocyte and epithelial cells.

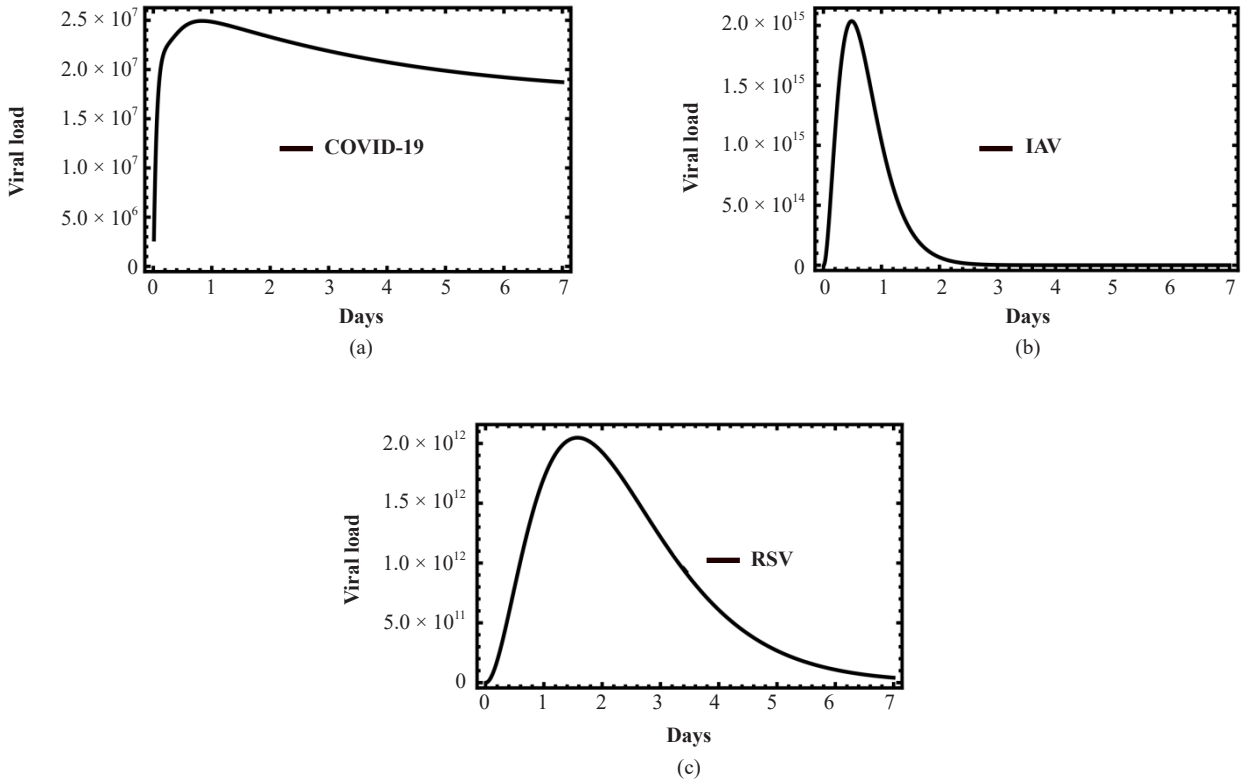

Figure 10. (a) SARS-CoV-2 viral load as a function of time. (b) IAV viral load as a function of time. (c) RSV viral load as a function of time. The three viruses simultaneously infect the target cells and SARS-CoV-2 also targets the lymphocytes as secondary host cells. In the figures, $T(0)$ = 10,000,000, $V_1(0)$ = 100,000, $V_2(0)$ = 100,000 and $V_3(0)$ = 100,000. As shown in the figures, when SARS-CoV-2, RSV, and IAV simultaneously infect the host cells, the cellular resources deplete fast. IAV exhibits the highest viral load in a short period, it then decays fast as it has a higher viral infection rate. RSV on the other hand has a higher infection rate than SARS-CoV-2. RSV also depicts a higher viral load than SARS-CoV-2.

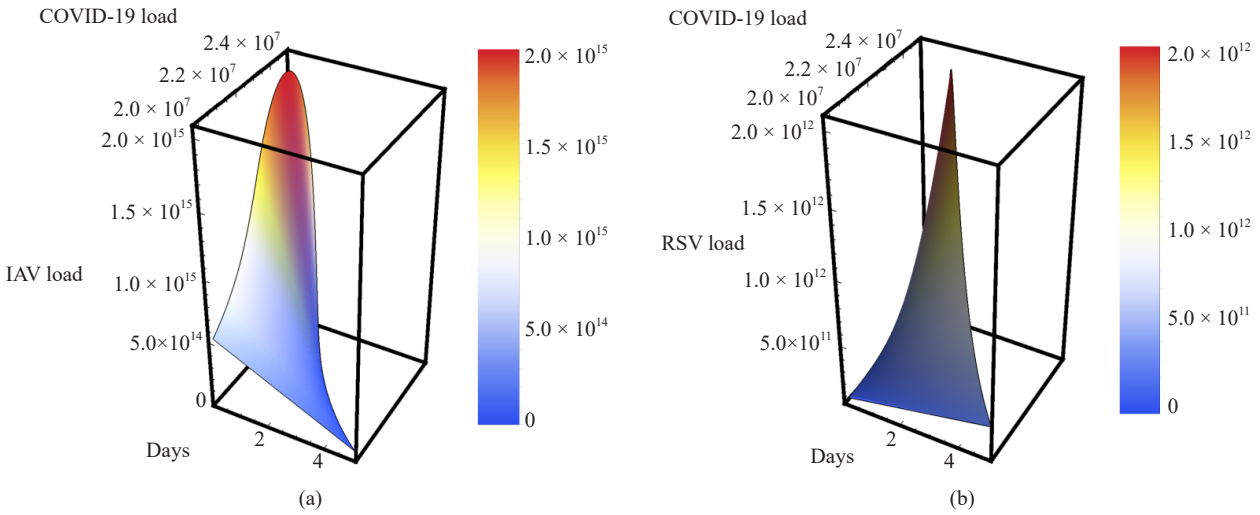

Figure 11. (a) IAV and SARS-CoV-2 as a function of time. (b) RSV and SARS-CoV-2 as a function of time.

SARS-CoV-2 by targeting the lymphocytes as secondary host cells, not only it gets an additional reproduction medium, but it also improves its survival rates since the depletion of lymphocytes weakens the host defense system. Our key finding is that since SARS-CoV-2 infects lymphocytes in addition to the epithelial cells, it exhibits a higher viral load in comparison to Section 2 (see Figure 6). As depicted in Figure 10a, 10b, and 10c, when SARS-CoV-2, RSV, and IAV simultaneously infect the host cells, the cellular resources deplete fast. IAV exhibits the highest viral load in a short period, it decays fast as it has a higher viral infection rate. RSV on the other hand has a higher infection rate than SARS-CoV-2. RSV also depicts a higher viral load than SARS-CoV-2. To get a clear understanding, we re-plotted Figure 10 three-dimensionally in Figures 11a, and 11b. In the figures, IAV and SARS-CoV-2 as well as RSV and SARS-CoV-2 as a function of time are plotted. The same figures are plotted by assuming the three viruses simultaneously infect the target cells and SARS-CoV-2 also targets the lymphocytes as secondary host cells. The initial host and viral load are fixed as $T(0) = 10{,}000{,}000$, $V_1(0) = 100{,}000$, $V_2(0) = 100{,}000$ and $V_3(0) = 100{,}000$.

The ratio of infectious cells π_1, π_2 and π_3 as a function of time as well as the ratio of varial load ζ_1, ζ_2 and ζ_3 as a function of time is studied when IAV delayed for five days and SARS-CoV-2 for one day after RSV establishes an infection. As shown in Figure 12a and 12b, RSV dominates the overall infections for a few days. After a few days, SARS-CoV-2 starts to depict a higher viral load. In the long time limit, the ratio of IAV becomes higher. We assume that only SARS-CoV-2 infects the lymphocytes. The lymphocyte load as a function of time is shown in Figure 13.

In Figure 14, we plot the ratio of SARS-CoV-2 viral load ζ_1 as a function of time and initial SARS-CoV-2 during simultaneous infection of SARS-CoV-2, IAV, and RSV. Once again, as depicted in Figure 14, SARS-CoV-2 has a competitive advantage over the other two viruses in a long time limit as it has the lowest viral reproduction rate. Even if an infection is over, a person can shed the virus for a longer period.

The plot for the ratio of IAV viral load ζ_2 as a function of time and initial SARS-CoV-2 inoculum during simultaneous infection of SARS-CoV-2, IAV, and RSV is depicted in Figure 15. Since IAV has the highest viral reproduction rate, it is highly competitive over a short time. In Figure 16, we plot the ratio of RSV viral load ζ_3 as a function of time and initial SARS-CoV-2 inoculum during simultaneous infection of SARS-CoV-2, IAV, and RSV. Once again, as depicted in Figure 16, the viral load ratio for RSV becomes dominant for an intermediate time. Here, we analyzed the viral load up to 200 days since viral shading persists for many days after symptom onset [44].

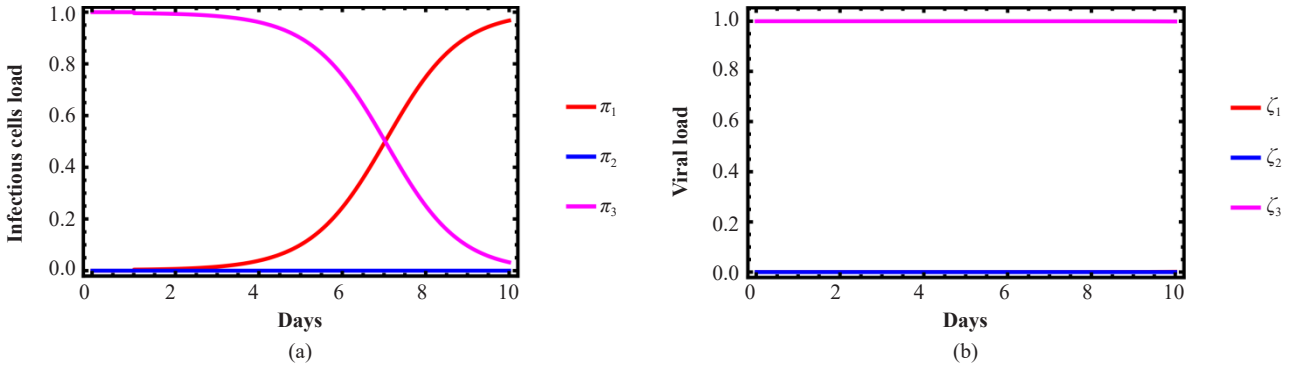

Figure 12. (a) The ratio of infectious cells π_1, π_2 and π_3 as a function of time. (b) The ratio of viral load ζ_1, ζ_2 and ζ_3 as a function of time when IAV is initiated five days after RSV establishes an infection and SARS-CoV-2 is initiated one day after RSV establishes an infection. As shown in the figures, RSV dominates the overall infections for a few days. After a few days, SARS-CoV-2 starts to depict a higher viral load. In the long time limit, the ratio of IAV becomes higher.

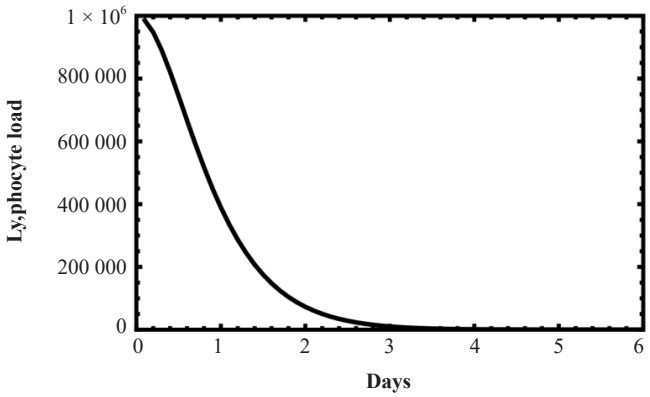

Figure 13. The lymphocyte load is a function of time when the three viruses simultaneously infect the target cells. The figure shows that the lymphocyte load decreases as a function of time.

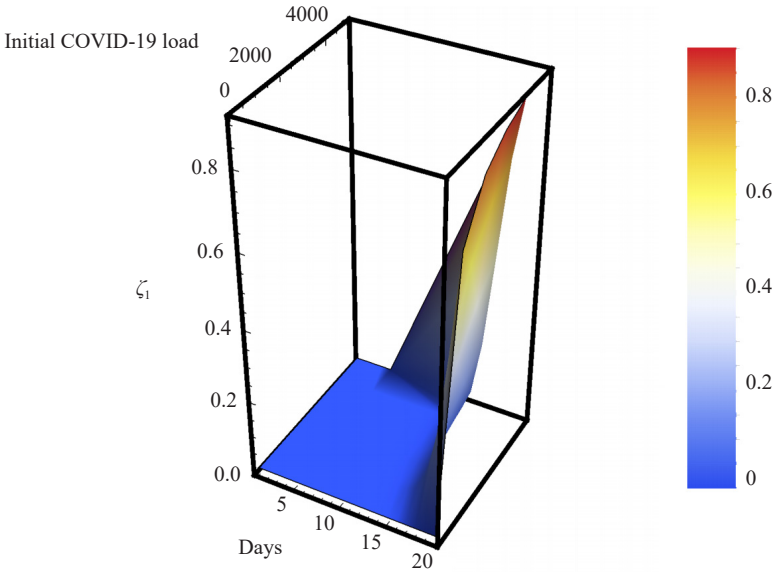

Figure 14. The ratio of SARS-CoV-2 varial load ζ_1 as a function of time and initial SARS-CoV-2 inoculum. The three viruses simultaneously infect the target cells and SARS-CoV-2 also targets the lymphocytes as secondary host cells. As depicted in the figures, SARS-CoV-2 has a competitive advantage over the other two viruses in a long time limit as it has the lowest viral reproduction rate.

The model system presented in this system only studies the viral production rate in the respiratory tract. The reported viral load might be considerably high since, unlike IAV and RSV, SARS-CoV-2 infects several organs. SARS-CoV-2, by infecting the lymphocytes, not only boosts its viral load but also hinders the immune response. Most importantly, even a smaller SARS-CoV-2 viral load can be associated with a higher mortality rate since it activates a cytokine storm. In the case of triple coinfection of the three viruses, the viruses directly interact through cellular resources, and they also indirectly interact via the immune response. The availability of vaccines as well as antiviral drugs alters the viral dynamics. If a patient is vaccinated for SARS-CoV-2, the virus becomes illuminated by the adaptive immune system. The remaining the other two viruses start to replicate and depending on their viral production rate, one of the viruses dominates the overall dynamics. On the other hand, if less virulent viruses establish an infection before the other two viruses, the virulent viruses will be out of the competition giving a survival advantage to the host. The implication of this study indicates that via artificially made non-virulent viruses, the infection dynamics can be manipulated.

Throughout this paper, the role of vaccination has not been considered. Our model system does not include the effect of cell regeneration. Regeneration of new target cells gives a competitive advantage to the virus which has the lowest replication rate. In this paper, it is assumed that only one virus can infect one cell. However, it is an experimental fact that superinfection with two or more viruses occurs. One can note that since viruses exhibit tropism, two different strains of a given virus may not have common target cells.

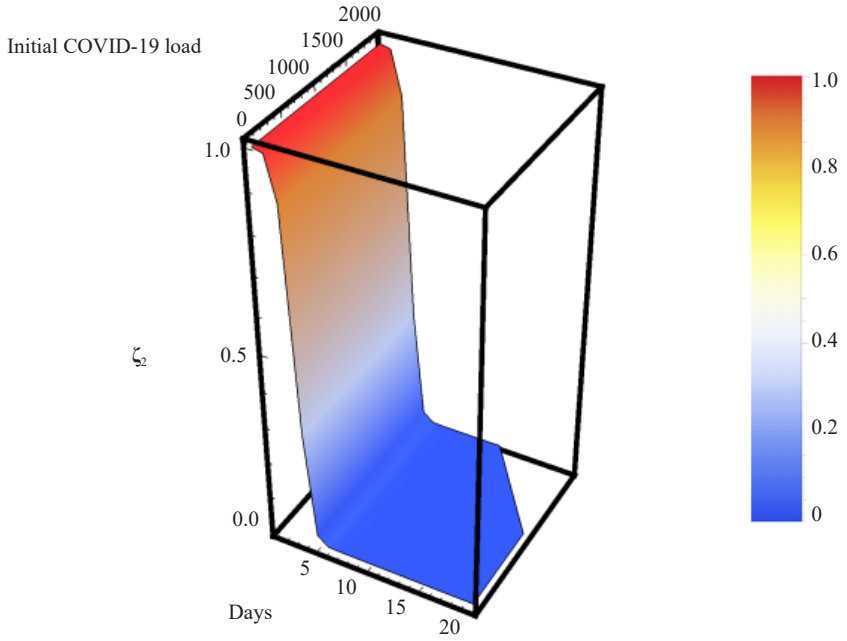

Figure 15. The ratio of IAV varial loads ζ_2 as a function of time and initial SARS-CoV-2 inoculum. The three viruses simultaneously infect the target cells and SARS-CoV-2 also targets the lymphocytes as secondary host cells.

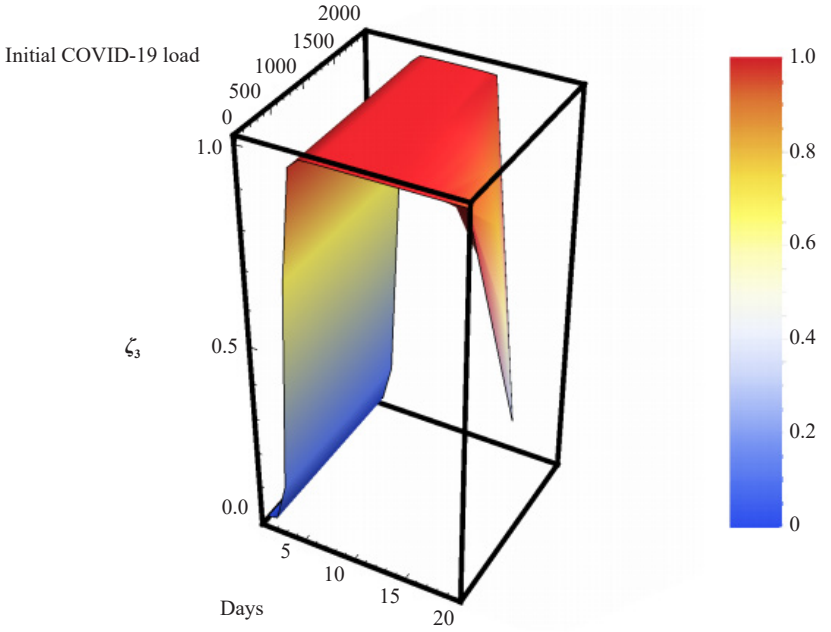

Figure 16. The ratio of RSV varial loads ζ_3 as a function of time and initial SARS-CoV-2 inoculum. The three viruses simultaneously infect the target cells and SARS-CoV-2 also targets the lymphocytes as secondary host cells.

5. Summary and conclusions

The dynamics of the virus for triple coinfection cases are studied via numerical simulations where SARS-CoV-2, IAV, and RSV infect the host cells. In case of a single infection, each virus can utilize the cellular resource without harsh competition. However, when these viruses concurrently infect the host cells, they interfere either synergically or destructively by competing for available resources. Since IAV has the highest infection rate at the cellular level, it dictates the length of the infection cascade. By infecting most of the cells, it reproduces fast yielding the highest viral load in a short period. On the contrary, SARS-CoV-2 has the lowest viral replication rate, and its viral load for SARS-CoV-2 declines slowly as a result, they become infectious for a longer period. The present study also suggests that the fast-growing virus dictates the overall dynamics by excluding all other slow-growing viruses in a relatively short period. However, in the longer time limit, the viruses which have a slower replication rate dominate the viral dynamics.

The coinfection dynamics are also dictated by the initial viral inoculum. Higher initial viral inoculum for the SARS-CoV-2 virus suppresses the growth of RSV and IAV since the SARS-CoV-2 virus depletes the cellular resources. A higher initial viral load facilitates more cellular infection when the infection starts. As time goes on, the fast-growing virus can infect more target cells. The timing of the infection is also a determinant factor. For instance, when the RSV and IAV infections are initiated after a few days of SARS-CoV-2 infection, SARS-CoV-2 dominates for a short period since it utilizes the available resources. However, the fast-growing virus (namely, IAV) quickly takes over and governs the overall dynamics for a long time limit. In the case of simultaneous infection of the three viruses, a higher viral load is exhibited than a single infection case which indicates that simultaneous infection with SARS-CoV-2, influenza A, and the syncytial virus can be associated with higher morbidity and mortality. SARS-CoV-2 is also known for targeting the lymphocytes as secondary host cells. As a result not only it gets an additional reproduction medium, but it also improves its survival rates since the depletion of lymphocytes weakens the host defense system. Our key finding indicates that, when lymphocytes as target cells are included in the model system, a higher viral load is observed.

When SARS-CoV-2, IAV, and RSV concurrently infect the host, the viruses interfere through the available resources as well as via the immune system. The viral dynamics is significantly influenced by the availability of vaccine and antiviral drugs. For the triple coinfection case, the SARS-CoV-2 virus becomes cleared by the adaptive immune system if a patient is vaccinated for SARS-CoV-2. The remaining the other two viruses start to replicate and depending on their viral production rate, one of the viruses dominates the overall dynamics. On the other hand, if less virulent

viruses establish an infection before the other two viruses, the virulent viruses will be out of the competition giving a survival advantage to the host. The implication of this study indicates that via artificially made non-virulent viruses, the infection dynamics can be manipulated. In conclusion, in this work, we present a simple model which not only serves as a basic tool for a better understanding of viral dynamics in vivo and in vitro but also helps in developing an effective therapeutic strategy.

Acknowledgments

I would like to thank Mulu Zebene and Blaynesh Bezabih for their constant encouragement.

Conflict of interest

The author declares no competing financial interest..

References

[1] Ouassou H, Kharchoufa L, Bouhrim M, Daoudi NE, Imtara H, Bencheikh N, et al. The Pathogenesis of coronavirus disease 2019 (COVID-19): Evaluation and prevention. *Journal of Immunology Research*. 2020; 2020: 1357983. Available from: https://doi.org/10.1155/2020/1357983.

[2] Anderson RM, Heesterbeek H, Klinkenberg D, Hollingsworth TD. How will country-based mitigation measures influence the course of the COVID-19 epidemic? *The Lancet.* 2020; 395(10228): 931-934. Available from: https://doi.org/10.1016/S0140-6736(20)30567-5.

[3] Davies NG, Kucharski AJ, Eggo RM, Gimma A, Edmunds WJ, Jombart T, et al. Effects of non-pharmaceutical interventions on COVID-19 cases, deaths, and demand for hospital services in the UK: A modelling study. *The Lancet Public Health.* 2020; 5(7): e375-385. Available from: https://doi.org/10.1016/S2468-2667(20)30133-X.

[4] Ferretti L, Wymant C, Kendall M, Zhao L, Nurtay A, Abeler-Dörner L, et al. Quantifying SARS-CoV-2 transmission suggests epidemic control with digital contact tracing. *Science.* 2020; 368(6491): eabb6936. Available from: https://doi.org/10.1126/science.abb6936.

[5] Kyrychko YN, Blyuss KB, Brovchenko I. Mathematical modelling of the dynamics and containment of COVID-19 in Ukraine. *Scientific Reports.* 2020; 10: 19662. Available from:https://doi.org/10.1038/s41598-020-76710-1.

[6] Du SQ, Yuan W. Mathematical modeling of interaction between innate and adaptive immune responses in COVID-19 and implications for viral pathogenesis. *Journal of Medical Virology.* 2020; 92(9): 1615-1628. Available from: https://doi.org/10.1002/jmv.25866.

[7] Hernandez-Vargas EA, Velasco-Hernandez JX. In-host mathematical modelling of COVID-19 in humans. *Annual Reviews in Control.* 2020; 50: 448-456. Available from: https://doi.org/10.1016/j.arcontrol.2020.09.006.

[8] Wang S, Pan Y, Wang Q, Miao H, Brown AN, Rong L. Modeling the viral dynamics of SARS-CoV-2 infection. *Mathematical Biosciences*. 2020; 328: 108438. Available from: https://doi.org/10.1016/j.mbs.2020.108438.

[9] Goto H, Ihira H, Morishita K, Tsuchiya M, Ohta K, Yumine N, et al. Enhanced growth of influenza A virus by coinfection with human parainfluenza virus type 2. *Medical Microbiology and Immunology.* 2016; 205: 209-218. Available from: https://doi.org/10.1007/s00430-015-0441-y.

[10] Shinjoh M, Omoe K, Saito N, Matsuo N, Nerome K. In vitro growth profiles of respiratory syncytial virus in the presence of influenza virus. *Acta Virologica*. 2000; 44(2): 91-97. PMID: 10989700. Available from: https://pubmed.ncbi.nlm.nih.gov/10989700/.

[11] Pinky L, Dobrovolny HM. Coinfections of the respiratory tract: viral competition for resources. *PloS One*. 2016; 11(5): e0155589. Available from: https://doi.org/10.1371/journal.pone.0155589.

[12] Goka EA, Vallely PJ, Mutton KJ, Klapper PE. Single, dual and multiple respiratory virus infections and risk of hospitalization and mortality. *Epidemiology & Infection.* 2015; 143(1): 37-47. Available from: https://doi.

org/10.1017/S0950268814000302.
[13] Martin ET, Fairchok MP, Stednick ZJ, Kuypers J, Englund JA. Epidemiology of multiple respiratory viruses in childcare attendees. *The Journal of Infectious Diseases*. 2013; 207(6): 982-989. Available from: https://doi.org/10.1093/infdis/jis934.
[14] Brand HK, de Groot R, Galama JM, Brouwer ML, Teuwen K, Hermans PW, et al. Infection with multiple viruses is not associated with increased disease severity in children with bronchiolitis. *Pediatric Pulmonology*. 2012; 47(4): 393-400. Available from: https://doi.org/10.1002/ppul.21552.
[15] Rotzén-Östlund M, Eriksson M, Tiveljung Lindell A, Allander T, Zweygberg Wirgart B, Grillner L. Children with multiple viral respiratory infections are older than those with single viruses. *Acta Paediatrica.* 2014; 103(1): 100-104. Available from: https://doi.org/10.1111/apa.12440.
[16] Martin ET, Kuypers J, Wald A, Englund JA. Multiple versus single virus respiratory infections: Viral load and clinical disease severity in hospitalized children. *Influenza and Other Respiratory Viruses.* 2012; 6(1): 71-77. Available from: https://doi.org/10.1111/j.1750-2659.2011.00265.x.
[17] Waner JL. Mixed viral infections: Detection and management. *Clinical Microbiology Reviews.* 1994; 7(2):143-151. PMID: 8055464. Available from: https://doi.org/10.1128/cmr.7.2.143.
[18] Zitzmann C, Kaderali L. Mathematical analysis of viral replication dynamics and antiviral treatment strategies: From basic models to age-based multi-scale modeling. *Frontiers in Microbiology.* 2018; 9: 1546. Available from: https://doi.org/10.3389/fmicb.2018.01546.
[19] Wang Y, Liu J, Liu L. Viral dynamics of an HIV model with latent infection incorporating antiretroviral therapy. *Advances in Difference Equations*. 2016; 2016(1): 1-15. Available from: https://doi.org/10.1186/s13662-016-0952-x.
[20] Chen SS, Cheng CY, Takeuchi Y. Stability analysis in delayed within-host viral dynamics with both viral and cellular infections. *Journal of Mathematical Analysis and Applications.* 2016; 442(2): 642-672. Available from: https://doi.org/10.1016/j.jmaa.2016.05.003.
[21] Perelson AS, Kirschner DE, De Boer R. Dynamics of HIV infection of $CD4^+$ T cells. *Mathematical Biosciences.* 1993; 114(1): 81-125. Available from: https://doi.org/10.1016/0025-5564(93)90043-A.
[22] Perelson AS, Neumann AU, Markowitz M, Leonard JM, Ho DD. HIV-1 dynamics in vivo: Virion clearance rate, infected cell life-span, and viral generation time. *Science.* 1996; 271(5255): 1582-1586. Available from: https://doi.org/10.1126/science.271.5255.1582.
[23] Perelson AS, Essunger P, Cao Y, Vesanen M, Hurley A, Saksela K, et al. Decay characteristics of HIV-1-infected compartments during combination therapy. *Nature.* 1997; 387: 188-191. Available from: https://doi.org/10.1038/387188a0.
[24] Ho DD, Neumann AU, Perelson AS, Chen W, Leonard JM, Markowitz M. Rapid turnover of plasma virions and CD4 lymphocytes in HIV-1 infection. *Nature.* 1995; 373(6510): 123-126. Available from: https://doi.org/10.1038/373123a.
[25] Bonhoeffer S, May RM, Shaw GM, Nowak MA. Virus dynamics and drug therapy. *Proceedings of the National Academy of Sciences.* 1997; 94(13): 6971-6976. Available from: https://doi.org/10.1073/pnas.94.13.6971.
[26] Stafford MA, Corey L, Cao Y, Daar ES, Ho DD, Perelson AS. Modeling plasma virus concentration during primary HIV infection. *Journal of Theoretical Biology.* 2000; 203(3): 285-301. Available from: https://doi.org/10.1006/jtbi.2000.1076.
[27] Wei X, Ghosh SK, Taylor ME, Johnson VA, Emini EA, Deutsch P, et al. Viral dynamics in human immunodeficiency virus type 1 infection. *Nature.* 1995; 373(6510): 117-122. Available from: https://doi.org/10.1038/373117a0.
[28] Wodarz D, Nowak MA. Mathematical models of HIV pathogenesis and treatment. *BioEssays.* 2002; 24(12): 1178-1187. Available from: https://doi.org/10.1002/bies.10196.
[29] Din A, Li Y, Khan T, Zaman G. Mathematical analysis of spread and control of the novel corona virus (COVID-19) in China. *Chaos, Solitons & Fractals.* 2020; 141: 110286. Available from: https://doi.org/10.1016/j.chaos.2020.110286.
[30] Din A, Li Y, Khan FM, Khan ZU, Liu P. On Analysis of fractional order mathematical model of Hepatitis B using Atangana-Baleanu Caputo (ABC) derivative. *Fractals*. 2022; 30(01): 2240017. Available from: https://doi.

org/10.1142/S0218348X22400175.
[31] Din A, Li Y, Yusuf A, Ali AI. Caputo type fractional operator applied to Hepatitis B system. *Fractals*. 2022; 30(1): 2240023. Available from: https://doi.org/10.1142/S0218348X22400230.
[32] Din A. The stochastic bifurcation analysis and stochastic delayed optimal control for epidemic model with general incidence function. *Chaos*. 2021; 31(12): 123101. Available from: https://doi.org/10.1063/5.0063050.
[33] Graw F, Perelson AS. Modeling viral spread. *Annual Review of Virology.* 2016; 3: 555-572. https://doi.org/10.1146/annurevvirology-110615-042249. Available from: https://doi.org/10.1146/annurev-virology-110615-042249.
[34] Neumann AU, Lam NP, Dahari H, Gretch DR, Wiley TE, Layden TJ, et al. Hepatitis C viral dynamics in vivo and the antiviral efficacy of interferon-α therapy. *Science.* 1998; 282(5386): 103-107. Available from: https://doi.org/10.1126/science.282.5386.103.
[35] Dahari H, Lo A, Ribeiro RM, Perelson AS. Modeling hepatitis C virus dynamics: Liver regeneration and critical drug efficacy. *Journal of Theoretical Biology.* 2007; 247(2): 371-381. Available from: https://doi.org/10.1016/j.jtbi.2007.03.006.
[36] Nowak MA, Bonhoeffer S, Hill AM, Boehme R, Thomas HC, McDade H. Viral dynamics in hepatitis B virus infection. *Proceedings of the National Academy of Sciences.* 1996; 93(9): 4398-4402. Available from: https://doi.org/10.1073/pnas.93.9.4398.
[37] Lai X, Zou X. Modeling cell-to-cell spread of HIV-1 with logistic target cell growth. *Journal of Mathematical Analysis and Applications*. 2015; 426(1): 563-584. Available from: https://doi.org/10.1016/j.jmaa.2014.10.086.
[38] Li F, Wang J. Analysis of an HIV infection model with logistic target-cell growth and cell-to-cell transmission. *Chaos, Solitons & Fractals.* 2015; 81: 136-145. Available from: https://doi.org/10.1016/j.chaos.2015.09.003.
[39] Wang J, Lang J, Zou X. Analysis of an age structured HIV infection model with virus-to-cell infection and cell-to-cell transmission. *Nonlinear Analysis: Real World Applications*. 2017; 34: 75-96. Available from: https://doi.org/10.1016/j.nonrwa.2016.08.001.
[40] Hadjichrysanthou C, Cauët E, Lawrence E, Vegvari C, De Wolf F, Anderson RM. Understanding the within-host dynamics of influenza A virus: From theory to clinical implications. *Journal of The Royal Society Interface.* 2016; 13(119): 20160289. Available from: https://doi.org/10.1098/rsif.2016.0289.
[41] Hernandez-Vargas EA, Wilk E, Canini L, Toapanta FR, Binder SC, Uvarovskii A, et al. Effects of aging on influenza virus infection dynamics. *Journal of Virology.* 2014; 88(8): 4123-4131. Available from: https://doi.org/10.1128/JVI.03644-13.
[42] Chowdhury SM, Chowdhury JT, Ahmed SF, Agarwal P, Badruddin IA, Kamangar S. Mathematical modelling of COVID-19 disease dynamics: Interaction between immune system and SARS-CoV-2 within host. *AIMS Mathematics.* 2022; 7(2): 2618-2133. Available from: https://doi.org/10.3934/math.2022147.
[43] Ojosnegros S, Beerenwinkel N, Antal T, Nowak MA, Escarmís C, Domingo E. Competition-colonization dynamics in an RNA virus. *Proceedings of the National Academy of Sciences*. 2010; 107(5): 2108-2112. Available from: https://doi.org/10.1073/pnas.0909787107.
[44] Li J, Zhang L, Liu B, Song D. Case report: Viral shedding for 60 days in a woman with COVID-19. *The American Journal of Tropical Medicine and Hygiene.* 2020; 102(6): 1210-1213. Available from: https://doi.org/10.4269/ajtmh.20-0275.